JOURNAL OF MATERIALS SCIENCE 30 (1995) 3050–3056

Anisotropic plastic and elastic deformation in highly textured superconducting (Bi, Pb)$_2$ Sr$_2$ Ca$_2$ Cu$_3$O$_x$ ceramics

JIE LUO, R. STEVENS
School of Materials, University of Leeds, Leeds LS2 9JT, UK
WAI LO, A.M. CAMPBELL
IRC in Superconductivity, University of Cambridge CB3 OHE, UK

A highly textured (Bi, Pb)$_2$Sr$_2$Ca$_2$Cu$_3$O$_x$ superconductor has been prepared and the hardness, deformation and microcracking of the material explored using Vickers indentation. The present study has investigated the hardness anisotropy of the highly textured material on cross-sections of the specimen which have been chosen to give specific low-index orientations. The hardness was found to decrease as the indentation rotated from 0° (a diagonal of the indent parallel to the direction of the texturing) to 45° (the angle between a diagonal of the indent and the direction of the texturing). The square shape of the indent also changed with rotation from 0° to 45°. The hardness anisotropy has been attributed to the influence of elastic and plastic anisotropy in the polycrystalline materials. In addition, a weakness in the grain-boundary bonding results in the movement of adjacent grains by a sliding mechanism which dominated the indentation anisotropy effect. The presence of microcracking in the grain and at the grain boundary was found to affect the hardness anisotropy.

1. Introduction

The scientific and technological importance of a detailed study of the elastic and plastic deformation mechanisms of (Bi,Pb)$_2$Sr$_2$Ca$_2$Cu$_3$O$_x$ is clearly apparent. Mechanical deformation of the (Bi,Pb)$_2$Sr$_2$Ca$_2$Cu$_3$O$_x$ superconductor grains is a commonly used processing technique to achieve texturing and densification in this material, either in the form of bulk materials [1–10] or tapes [11–23]. Furthermore, stressing of the ceramic material in the superconducting state invariably arises when an electric current passes through the material in the presence of an external magnetic field due to the appearance of Lorentz forces acting on the magnetic flux lines in the material. Consequently, the material can either be deformed elastically or plastically. This situation where the ceramic is highly stressed could occur even more readily for the case of silver-clad (Bi,Pb)$_2$Sr$_2$Ca$_2$Cu$_3$O$_x$ tapes, where the thickness of the superconductor cores is usually in the range 20–100 μm, yet is capable of carrying a high superconducting current. Deformation of such small cross-section fragile tapes can also occur if they are inappropriately handled.

The mechanical properties of bulk (Bi,Pb)$_2$Sr$_2$Ca$_2$Cu$_3$O$_x$ superconductor, as reported in the literature, can be summarized as a low elastic modulus [24, 25], low yield stress'[26] and a high degree of brittleness (because the ratio of hardness to elastic modulus is low [26]). Plastic deformation in this material has been reported before fracture [27–29]. A study of Vickers indentation on highly textured materials has also confirmed that the bonding between the grains along their lattice *ab*-planes is particularly weak such that intergranular sliding and crack formation can occur preferentially [26]. However, little information concerning the anisotropy of elastic and plastic deformation due to the texturing of the (Bi,Pb)$_2$Sr$_2$Ca$_2$Cu$_3$O$_x$ superconducting grains is available in the reported literature, even though such data are important to a full understanding of the mechanical properties of this material. This is partially due to the fact that it is difficult to fabricate highly textured material with appropriate large dimensions in order that compliance analysis can be carried out. In this respect, it has been demonstrated that Vickers indentation testing is a useful tool to probe the mechanical properties of this brittle material because the requirement for large specimens is relaxed.

The present study has concentrated on revealing the anisotropic elastic and plastic deformation mechanisms in highly textured (Bi,Pb)$_2$Sr$_2$Ca$_2$Cu$_3$O$_x$ superconducting ceramics using Vickers indentation measurements. The indents and the accompanying damage as induced by the indentation process has been examined using high-resolution scanning electron microscopy (SEM). The deformation anisotropy, as quantified by the Vickers hardness and dimensions

0022–2461

of the indents, is explained in terms of the observed damage mechanisms.

2. Experimental procedure

The preparation procedure for the specimen used in the present study has been described elsewhere [1]. The $(Bi,Pb)_2Sr_2Ca_2Cu_3O_x$ grains in the specimen were aligned using a high magnetic field (6 T) at room temperature and the specimen densified before sintering using cold iso-static pressing. An examination of a polished cross-section of the specimen using high-resolution scanning electron microscopy (SEM) showed that the grains were highly textured, with the crystallographic c-axis of the grains orienting parallel to the direction of the applied magnetic field (the texturing direction) during magnetic alignment. A (0 0 2) pole distribution figure obtained using X-ray diffraction (XRD) texture goniometry confirmed that half the maximum intensity scattered within a misalignment angle of 21° [1, 26]. The bulk density of the specimen was estimated to be 83% of the theoretical density. The critical transition temperature of the specimen was 108 K and the transport critical current density at 77 K was 400 A cm^{-2}.

Vickers indentation measurements were carried out on a polished cross-section of the specimen (Fig. 1). The polished cross-section also contained the preferred direction of texturing, as indicated in Fig. 1, which in turn is perpendicular to the free surface. A change of relative orientation of the diagonals of the indent, (θ), with respect to the texturing direction was implemented by rotating the specimen stage. Although θ in this case was confined to be between 0° and 90°, the properties of the indents between 45° and 90° were understandably the same as those of the indents obtained between 0° and 45° due to the symmetry of the pyramidal indentor. The value of each θ was further confirmed by inspecting carefully the angle between one of the diagonals (BD in Fig. 1) of each indent and the specimen surface. A constant load of 1.5 N was used for all the indentations. The morphology of each of the indents was examined using high-resolution SEM. The lengths of the diagonals as well as two different sides of the indents (AB and BC in Fig. 1) were measured from each scanning electron micrograph. In order to seek an explanation for changes of the Vickers hardness as a function θ, the microstructures within the indents and around the indents were studied carefully using high-resolution SEM.

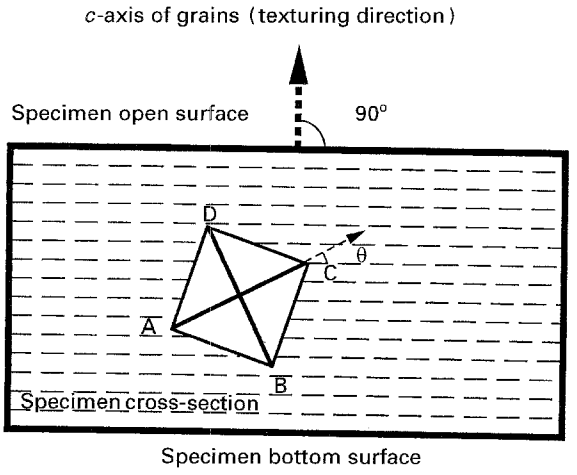

Figure 1 A schematic diagram illustrating the relationship between the texturing direction of the specimen and the orientation of the indentations.

3. Results and discussion

Fig. 2 shows the high-resolution scanning electron micrographs of three indents with θ equal to 10° 30° and 40°, respectively. In spite of the common feature that none of the indents is square, there is a clear difference in their indent geometry. The 10° indent is slightly rhomboid (Fig. 2a) whereas the 40° indent exhibits a nearly rectangular shape (Fig. 2b), and the shape of the 30° indent appears to lie between the two shapes. In addition, differences in the microstructures around the edges of the indents are also noticeable from the micrographs, suggesting the possible presence of multiple damage mechanisms caused by these indents.

A quantitative analysis of the difference in indent geometry is summarized by the Vickers hardness distribution with respect to changes of θ, as shown in Fig. 3. The Vickers hardness is calculated from the equation.

$$H_v = 1.83 \times 10^6 P/(BD)^2 (MPa) \quad (1)$$

where P is the indentation load which in this case is 1.5 N, and BD is the length of one of the indent diagonals (μm), as defined in Fig. 1. There is a pronounced variation of the value of H_v on rotation of the indentor: H_v is a minimum when θ is 45°, and its value is raised gradually when θ is either increased or decreased. The same trend is shared by the changes in the average Vickers hardness ($H_{v,av}$) with θ in Fig. 4, and $H_{v,av}$ is defined as:

$$H_{v,av} = 1.83 \times 10^6 P/[(AC + BD)/2]^2 \text{ (MPa)} \quad (2)$$

where AC is the second diagonal, defined in Fig. 1. In order to set an indicator for the deviation of the shapes of the indents from square geometry, the lengths of AB and BC, as defined in Fig. 1, are plotted in Fig. 5 as functions of θ. Both the lengths, AB and BC, change with θ. However, the change of the length of BC with an increase in θ is more pronounced so that the ratio AB /BC decreases as θ approaches 45°, consistent with a more rectangular geometry for the indent at orientations near 45°.

As the lengths of both AB and BC were measured after unloading, an important deduction to be made from the θ dependence of AB/BC is that the rate of elastic recovery in the indents along the texturing direction is lower than for the transverse perpendicular direction. Such an apparently texture-induced phenomenon can be correlated with the expected elastic modulus anisotropy of each individual $(Bi,Pb)_2Sr_2Ca_2Cu_3O_x$ grain in the specimen, resulting from nature of the bonding present in the layered lattice structure of this phase. However, elastic modulus data on the $(Bi,Pb)_2Sr_2Ca_2Cu_3O_x$ grains is

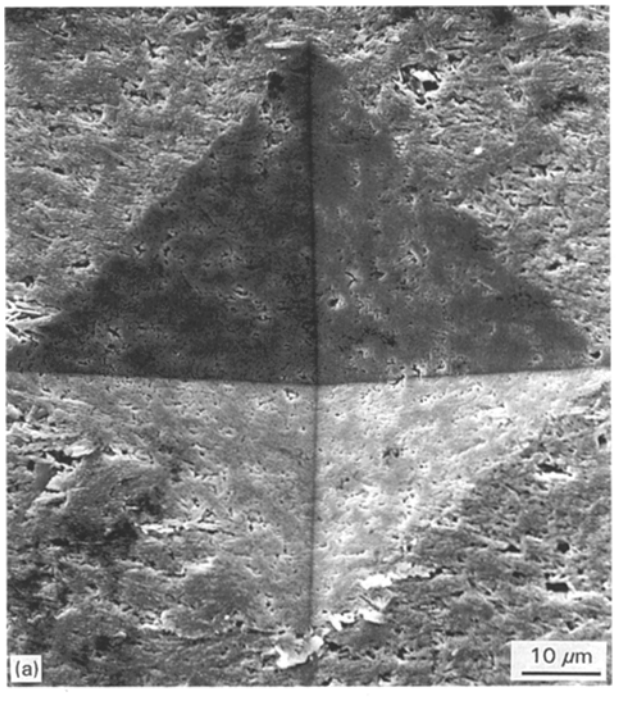

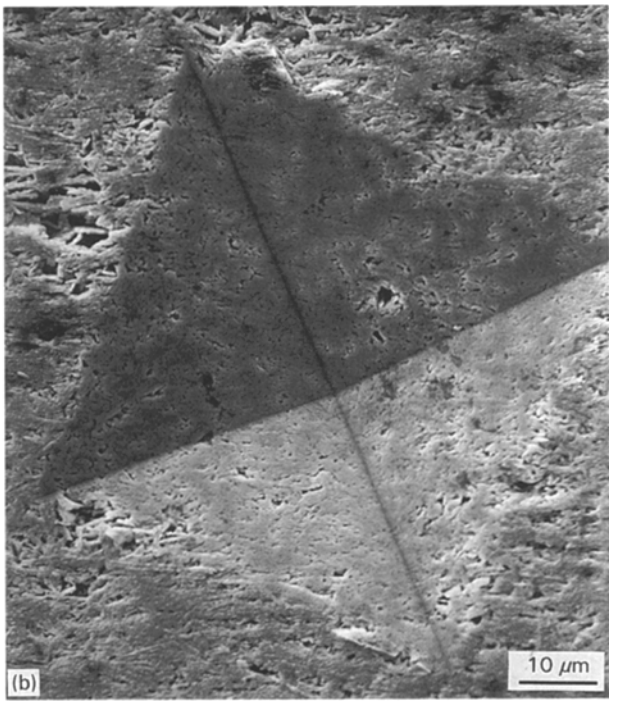

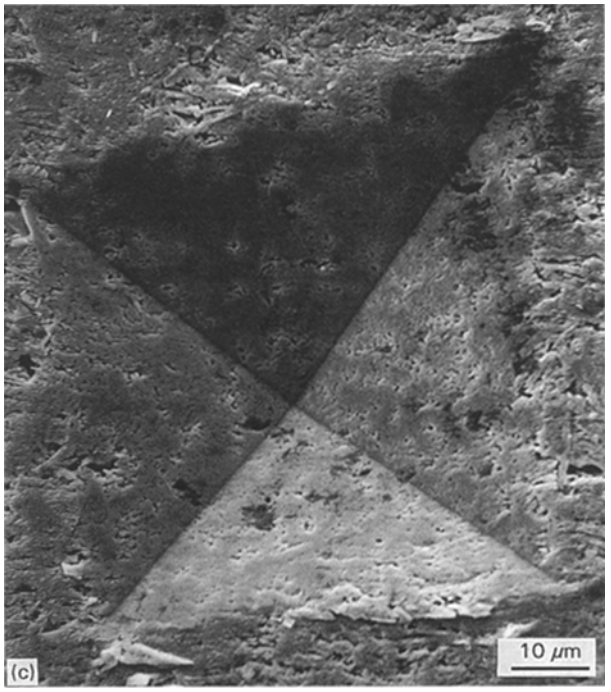

Figure 2 High-resolution scanning electron micrographs showing the morphologies of the indentations made at different angles relative to the texturing direction. Indents with θ = (a) 10°, (b) 30°, and (c) 40°.

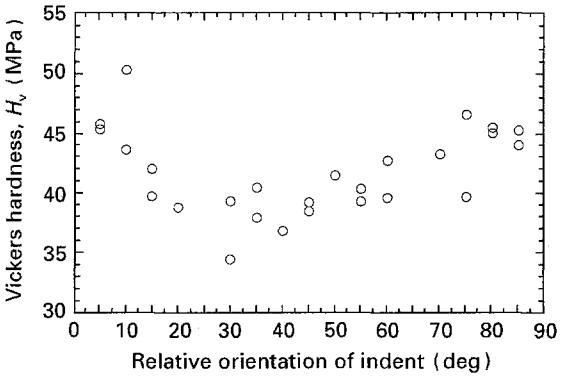

Figure 3 Orientation dependence of the Vickers hardness, (H_v).

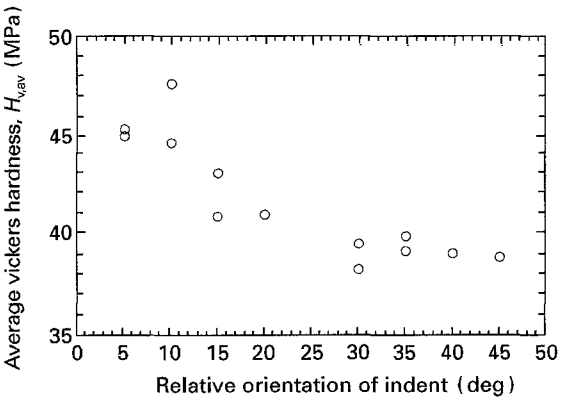

Figure 4 Orientation dependence of the average Vickers hardness, ($H_{v,av}$).

still to be reported because $(Bi,Pb)_2Sr_2Ca_2Cu_3O_x$ single crystals are as yet, unavailable. An indication of the anisotropy of the elastic modulus can only be sought from the elastic modulus obtained from crystals of a similar superconductor, $Bi_2Sr_2CaCu_2O_y$, which also has a layered lattice structure. The elastic modulus on a lattice *ab*-plane of a $Bi_2Sr_2CaCu_2O_y$ crystal at room temperature has been shown to the high, whereas the elastic modulus along the lattice *c*-axis is low and the elastic modulus at angles inclined both to the *ab*-plane and *c*-axis lies in between [24]. On the other hand, as the geometry of the deformation zone under an indent on a highly textured specimen has been shown to be semi-spherical [26], it is reasonable to assume the existence of an approximately semi-spherical stress distribution beneath the indent on loading. Based on this pattern of stress distribution, the direction of the compressive stress acting on the grains can be visualized as changing form point to point on the semi-sphere, with those grains nearer to the bottom and top

surfaces of the specimen being stressed along the c-axis and the others being stressed at an angle to the c-axis. The elastic recovery on unloading is thus anisotropic, due to the anisotropy of the elastic modulus of the grains, and the contraction on unloading along the c-axis is the least. A change of indent shape with respect to θ would thus be predicted.

A complementary explanation of the elastic recovery anisotropy is a consequence of the anisotropy of the ratio of the elastic and plastic deformation induced by the indent in the surrounding material on loading. The nature of the "plastic " deformation can be obtained by an inspection of the microstructure of the material around the indents. Fig. 6 shows the high-resolution scanning electron micrographs taken from the impressed area and in the vicinity of the indents made under different angles with respect to the texturing direction. Fig. 6a shows the microstructure of the grains near a diagonal within the impressed area of a 0° indent. A step-like structure between the grains is apparent, suggesting that the bonding between the grains along their *ab*-planes is sufficiently weak that intergranular sliding occurs once the grains are stressed. Such a conclusion is consistent with the results of a previous study on this material [26]. On the edge of the 0° indent, intergranular sliding as well as cracking along the intergranular *ab*-planes can be observed. As θ is increased, more and more grains are fractured along the BC side, although the fracturing process is deflected by the preferential cracking taking place along the weakly bonded grain boundaries (Fig. 6c). Unlike BC, relaxation of the compressive stress along AB has generated further intergranular sliding and the formation of pile-ups (Fig. 6c). Further differentiation of the damage mechanisms along these two sides continued when θ approached 45°. Along BC, the damage is predominantly transgranular fracturing and intergranular cracking (Fig. 6e), so that the high strain energy due to grain bending can be released. On the other hand, the damage along AB is mainly long-range grain sliding and pile-up formation (Fig. 6f). Such long-range damage along the AB axis suggests that the yield stress in this direction is lower than the yield stress along BC. This deduction is credible because the bonding strength between the grains is likely to be much weaker than the strength of

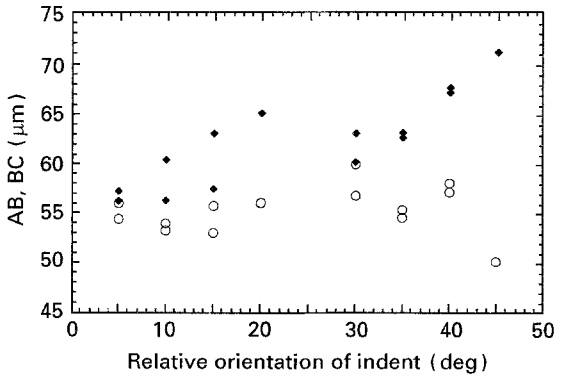

Figure 5 Orientation dependence of two sides of the indentations. (○) AB, and (◆) BC.

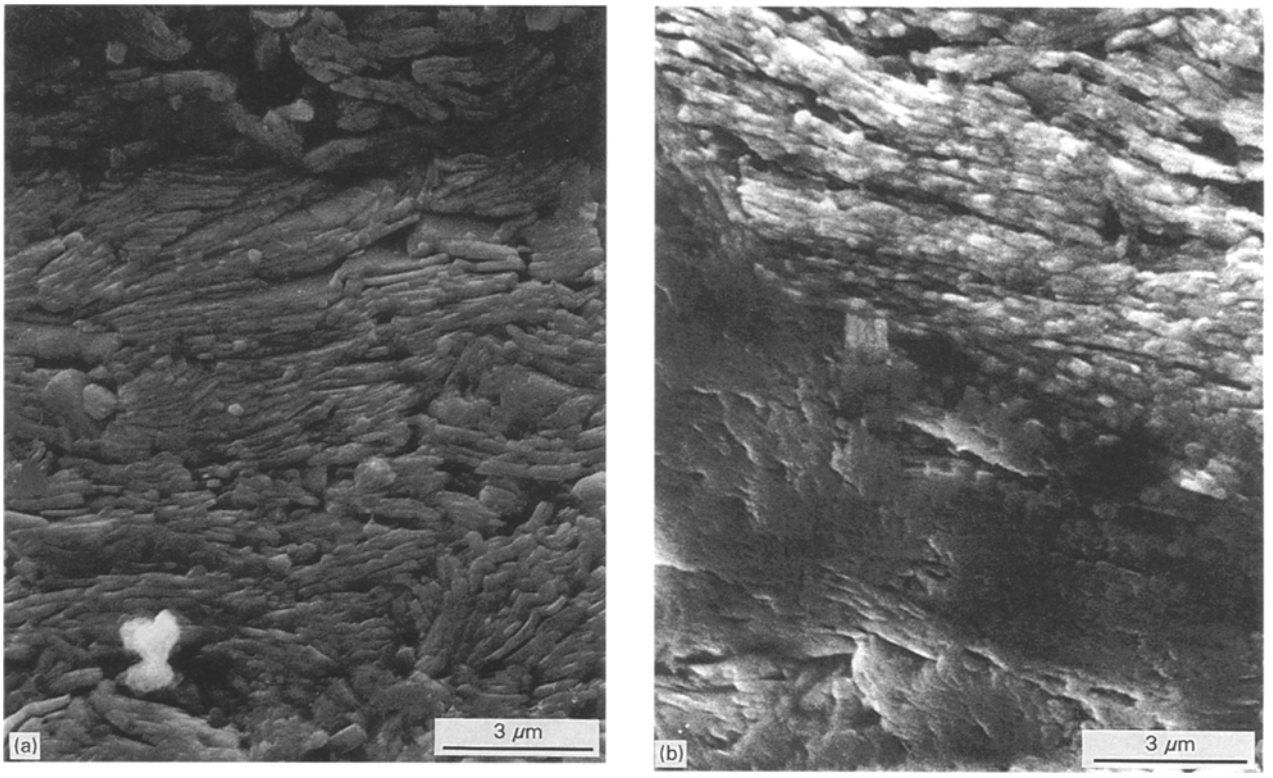

Figure 6 High-resolution scanning electron micrographs showing various kinds of damage to the specimen caused by the indentor. (a) Step-like structure between the grains near one of the diagonals in the $\theta = 0°$ indent, showing a weak bonding between the *ab*-planes of the grains; (b) intergranular cracking observed near one of the sides of a $\theta = 0°$ indent; (c) intergranular cracking and transgranular fracturing along BC of a $\theta = 30°$ indent; (d) intergranular sliding and short range pile-up formation along AB of a $\theta = 30°$ indent; (e) intergranular cracking and transgranular fracturing along BC of a $\theta = 40°$ indent; and (f) intergranular sliding and long range pile-up formation along AB of a $\theta = 40°$ indent.

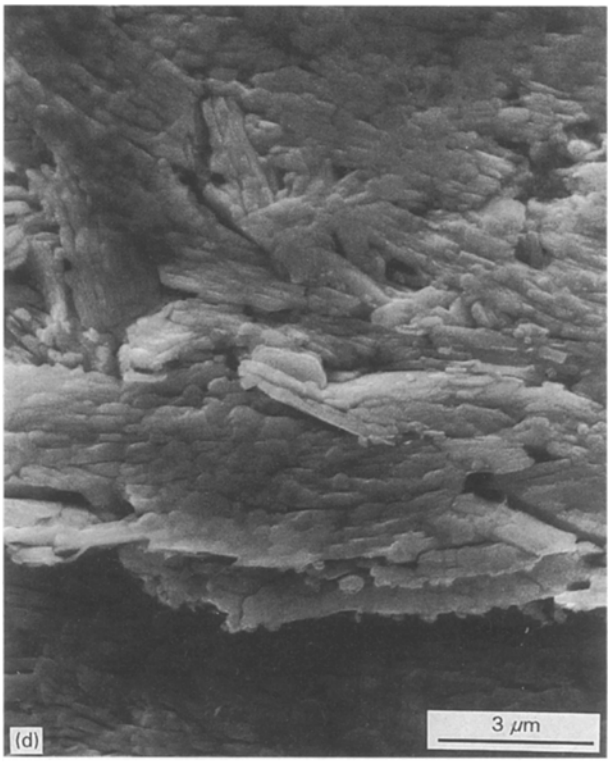

Figure 6 (contd).

each individual grain. As the elastic recovery process is dependent on the stress at which fracture is initiated, the elastic recovery of AB should therefore decrease, whereas the elastic recovery along BC should increase, when θ varies from 0° to 45°.

Although both H_v and $H_{v,av}$ are closely related to elastic recovery, an analysis of the anisotropy in H_v and $H_{v,av}$ should take into account the nature of the different damage mechanisms as θ is changed. In addition, as the fracture stress, as well as the elastic modulus of the present material is low [24, 26], the mechanical energy from the indentor on loading is also likely to be dissipated in the form of non-recoverable specimen damage rather than elastic straining. The operative damage mechanism could therefore play an important role in explaining the anisotropy in H_v and $H_{v,av}$. The micro and macrostructural damage recorded in the scanning electron micrograph from indents are summarized in the schematic diagrams in Fig. 7 for the two extreme cases, θ equal to 0° and 45°.

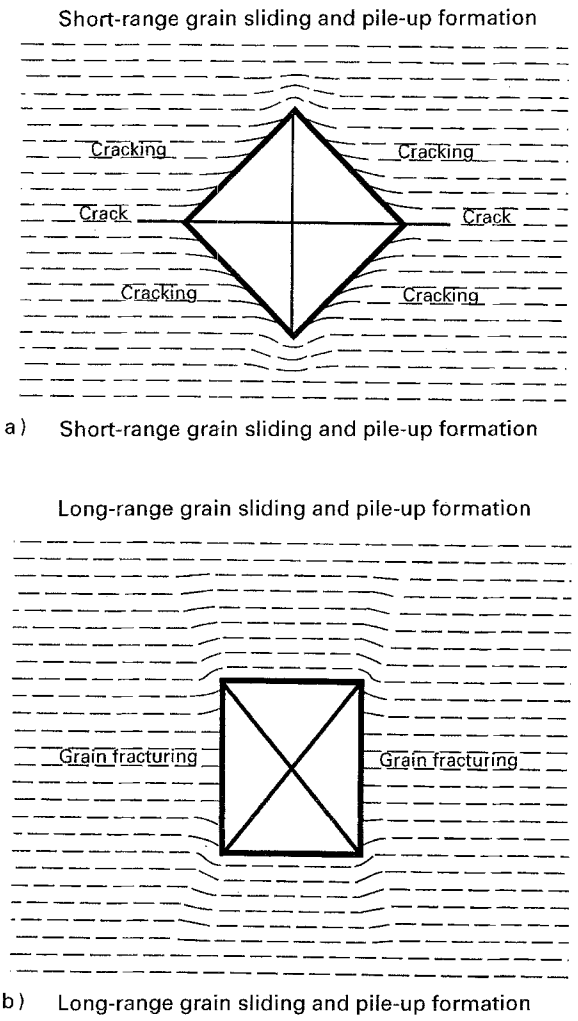

Figure 7 Schematic diagrams summarizing different damage mechanisms of the specimen as observed from the two extreme cases of the indentation rotation. θ = (*a*) 0°, and (b) 45°.

In the former case, intergranular cracking and grain fracturing occur substantially around the sides of the indent, over a short range (about 10% of the length of AB) for the intergranular sliding and pile-up formation near both B and D (Fig. 7a). In comparison, it has been frequently observed for the case of the 45° indents, that the range of intergranular sliding and pile-up formation along the whole of AB can be as much as 50% of the length of AB, while the nature of damage predominant along BC is intergranular cracking and grain fracturing, decreasing the opportunity for extensive elastic recovery on BC (Fig. 7b). The specimen is thus more "deformable" when θ is 45°, and the hardness for $\theta = 45°$ is lower than the hardness of $\theta = 0°$. Correspondingly, in view of the increase in the degree of grain sliding and pile-up formation along AB as the θ changes from 0° to 45°, the decreases in both H_v and $H_{v,av}$ can be appreciated.

In the above analysis of both the elastic and non-elastic properties of the $(Bi,Pb)_2Sr_2Ca_2Cu_3O_x$ specimen, the reasoning is based on the assumption that the specimen is fully dense and that grain alignment in the specimen is complete. The features of the real $(Bi,Pb)_2Sr_2Ca_2Cu_3O_x$ specimen naturally deviate from this assumption, as described in the previous text. Densification beneath the indents does occur, decreasing the apparent hardness, and the effect of such densification could cause a greater decrease in hardness in the *bc* plane due to grain sliding and grain bending [26]. However, the operative mechanisms responsible for the anistropic elastic and plastic deformations, such as grain deformation, sliding, pile-up and cracking, should be the same for a fully dense material with perfect alignment of the individual crystals.

4. Conclusion

Hardness anisotropy of a highly textured $(Bi,Pb)_2Sr_2Ca_2Cu_3O_x$ superconducting ceramic has been measured on the cross-section surface which contains texturing. The maximum hardness occurs when a diagonal of the indent is parallel to the grain orientation, and the hardness decreases as the indent diagonal shifts away from the line of texturing to a minimum when the angle between the diagonal and the direction of the grain texturing is about 45°. The shape of the square indentation also changes, the maximum deviation also observed at 45°.

The factors shown to cause the hardness anisotropy include the elastic and plastic anisotropy of the textured materials. Interfacial sliding of adjacent grains dominated the anisotropy behaviour and change in shape of the indentation. Grain cracking and intergranular cracking have been shown to relieve some strain energy and to decrease the hardness, affecting the anisotropy. The cracking is also dependent on the indent orientation. At 45°, the grain cracking is at its most serious on the indent edge which is perpendicular to the direction of grain orientation, while damage along the indent edge parallel to the grain orientation is dominated by grain sliding. At other rotations, both the grain cracking and grain sliding occur. Pile-up damage is more obvious at the indent corners.

Acknowledgement

One of the authors (Wai Lo) acknowledges the financial support from Croucher Foundation in the form of a Research Fellowship.

Refrences

1. WAI LO, R. STEVENS, R. DOYLE, A. M. CAMPBELL and W. Y. LIANG, *J. Mater. Res.* Submitted.
2. WAI LO, D.N. ZHENG, B.A. GLOWACKI and A. M. CAMPBELL, *J. Mater. Sci.* **29** (1994) 3897.
3. H. IKEDA, R. YOSHIZAKI, K, YOSHIKAWA and N. TOMITA, *Jpn J. Appl. Phys.* **29** (1990) L430.
4. N. MURAYAMA, E. SUDO, M. AWANO, K. KANI and Y. TORRI, *ibid* **27** (1988) L1856.
5. T. UZUMAKI, K. YAMANAKA, N. KAMEHARA and K. NIWA, *Appl. Phys. Lett.* **54** (1989) 2253.
6. T. ASANO, Y. TANAKA, M. FUKUTOMI, K. JIKIHARA and H. MAEDA, *Jpn. J. Appl. Phys.* **28** (1989) L595.
7. X. YANG and T.K. CHAKI, *Supercond. Sci. Technol.* **6** (1993) 269.
8. *Idem, ibid.* **6** (1993) 343.
9. R. J. ASARO, S. AHZI, W. BLUMENTHAL and A. DIGIOVANNI, *Philos. Mag.* **66** (1992) 517.
10. G. STEINLAGE, R. ROEDER, K. TRUMBLE, K. BOWMAN, S. LI and M. MCELFRSH, *J. Mater. Res.* **9** (1994) 833.

11. A. PERIN, G. GRASSO, M. DAUMLING, B. HENSEL, E. WALKER and R. FLUKIGER, *Phys. C* **216** (1993) 339.
12. M. UEYAMA, T. HITAKA, T. KATO and K. SATO, *Jpn J. Appl. Phys.* **30** (1991) L1384.
13. Y. IKENO, K. DOI, Y. KAMISADA, K. HAGASHI and T. OGAWA, in "Layered Superconductors: Fabrication, Properties and Applications" MRS Symposium Proceedings, Vol. 275, edited by D.T. Shaw, C.C. Tsuei, T.R. Schneider and Y. Shiohara (Materials Research Society, Pittsburgh, USA) p. 843.
14. D. SHI, S. SALEM-SUGUI, JR., Z. WANG, I.F. GOODRICH, S.X. DOU, H.K. LIU, Y.C. GUO and C.C. SORRELL, *Appl. Phys. Lett.* **59** (1991) 3171.
15. T. HIKATA, K. SATO and H. HELOSUYANAGI, *Jpn J. Appl. Phys.* **28** (1989) L82.
16. T. HIKATA, M. UEYAMA, H. MUKAI, and K. SATO, *Cryogenics* **30** (1990) 924.
17. J.M. YOO and K. MUKHERJEE, *Phys. C* **222** (1994) 241.
18. G. GRASSO, A. PERIN, B. HENSEL and R. FLUKIGER, *Phys. C.* **217** (1993) 335.
19. Q. LI, K. BRODERSEN, H.A. HJULER and T. FRELTOFT, *Phys. C.* **217** (1993) 360.
20. WAI LO and B.A. GLOWACKI, *Supercond. Sci. Technol.* **4** (1991) S361.
21. *Idem*, (in "High-Temperature Superconductors, Materials Aspects" edited by H. C. Freyhardt, T. Flukiger and M. Peuckert (Informationsgesellschaft, Verpag, 1991) p. 1005.
22. *Idem*, in " Layered Superconductors: Fabrication, Properties and Applications," MRS Symposium Proceedings Vol. 275, edited by D.T. Shaw, T.R. Schneider, C.C. Teuei and Y. Shiohara (MRS, Pittsburg, 1992) p. 729.
23. B.A. GLOWACKI and WAI LO in "Superconductivity: Materials Physics and Applications," edited B. Raveau, K. Wasa, R. Suerynarayanan (I.I.T.T, Gournay sur Marne, France) p. 299.
24. F.G. CHANG, P.J. FORD, G.A. SAUNDERS, J. Q. LI, D.P. ALMOND, B. CHAPMAN, M. CANKURTARAN, R.B. POEPPEL and K.C. GORETTA, *Supercond. Sci. Technol.* **6** (1993) 484.
25. M. MURALIDHAR, K. NANDA KISHORE, Y.V. RAMANA and V.H. BABU, *Mater. Sci. Eng.* **B13** (1992) 215.
26. WAI LO, A.M. CAMPBELL, JIE LUO and R. STEVENS, *J. Mater. Res.*, **10** (1995) 568.
27. C.Y. CHU, J.L. ROUBORT, NAN CHEN, A.C. BLONDO, D.S. KUPPERMAN and K.C. GORETTA, *Supercond. Sci. Technol.* **5** (1992) 306.
28. K.C. GORETTA, M.E. LOOMANS, L. J. MARTIN, J. JOO, R. B. POEPPLE and NAN CHEN, *Supercond. Sci. Technol* **6** (1993) 282.
29. N. MCN. ALFORD, T.W. BUTTON and J. D. BIRCHALL, *ibid.* **3** (1990) 1.

Received 18 October 1994
and accepted 20 January 1995